Adsorption of silver on cellobiose and cellulose studied with MIES, UPS, XPS and AFM

S. Dahle, J. Meuthen, W. Viöl & W. Maus-Friedrichs

Cellulose

ISSN 0969-0239
Volume 20
Number 5

Cellulose (2013) 20:2469-2480
DOI 10.1007/s10570-013-0009-1

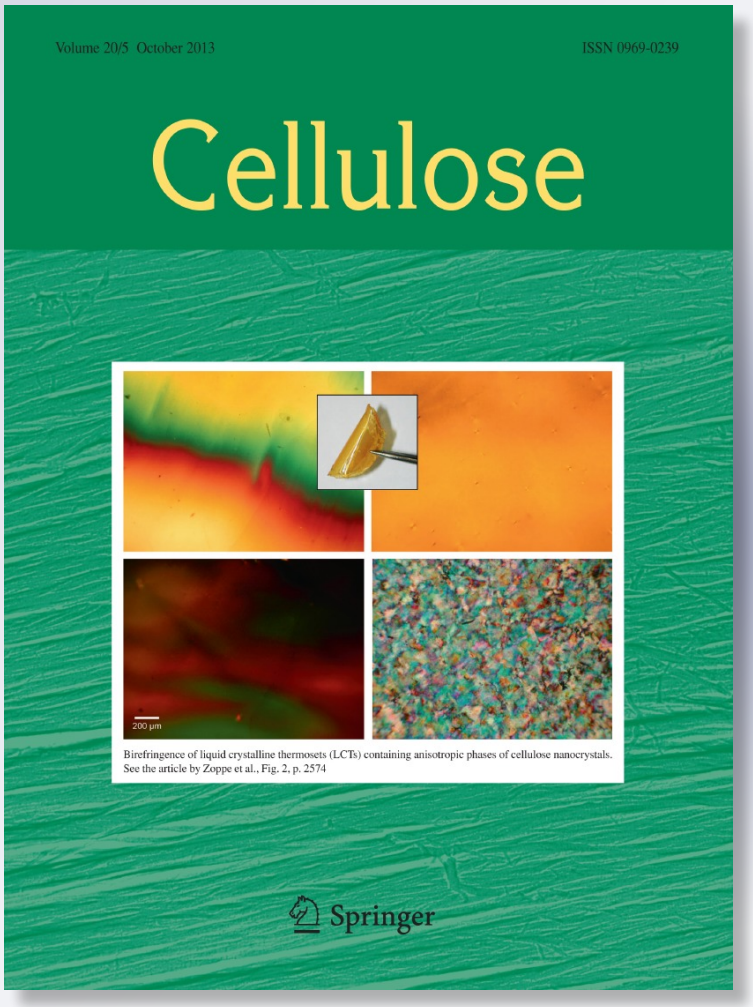

Springer

Cellulose (2013) 20:2469–2480
DOI 10.1007/s10570-013-0009-1

ORIGINAL PAPER

Adsorption of silver on cellobiose and cellulose studied with MIES, UPS, XPS and AFM

S. Dahle · J. Meuthen · W. Viöl · W. Maus-Friedrichs

Received: 27 April 2013 / Accepted: 24 July 2013 / Published online: 4 August 2013

Abstract Metastable induced electron spectroscopy, ultraviolet photoelectron spectroscopy and X-ray photoelectron spectroscopy as well as atomic force microscopy were employed to study the adsorption of silver on cellulose as well as its precursor cellobiose. The formation of silver nanoparticles encapsulated by the organic film previously found for the monomer glucose is well reproduced for the dimer cellobiose. For the polymer cellulose on the other hand, no nanoparticle formation is found even though the surface is covered with silver atoms. No significant chemical interaction is found in any of these cases.

S. Dahle · J. Meuthen · W. Maus-Friedrichs
Institut für Energieforschung und Physikalische Technologien, Technische Universität Clausthal, Leibnizstrasse 4, 38678 Clausthal-Zellerfeld, Germany

S. Dahle · W. Viöl
Hochschule für Angewandte Wissenschaft und Kunst, Fakultät für Naturwissenschaften und Technik, Von-Ossietzky-Straße 99, 37085 Göttingen, Germany

W. Viöl
Anwendungszentrum für Plasma und Photonic APP, Fraunhofer-Institut für Schicht-und Oberflächentechnik IST, Von-Ossietzky-Straße 99, 37085 Göttingen, Germany

W. Maus-Friedrichs (✉)
Clausthaler Zentrum für Materialtechnik, Technische Universität Clausthal, Leibnizstrasse 4, 38678 Clausthal-Zellerfeld, Germany
e-mail: w.maus-friedrichs@pe.tu-clausthal.de

Keywords Metastable induced electron spectroscopy · Ultraviolet photoelectron spectroscopy · X-ray photoelectron spectroscopy · Atomic force microscopy

Introduction

A variety of applications implement the adsorption of silver, such as corrosion protection, RF shielding, reflective coatings, and many more. Out of these, especially silver nanoparticle coatings showed outstanding functionality and thus gained much importance over the past 20 years. These silver nanoparticles are known e.g. to enhance the efficiency of organic light emitting devices (Yang et al. 2009) or possess outstanding antibacterial properties (Lok et al. 2006; Ilic et al. 2010; El-Shishtawy et al. 2011; Xue et al. 2012). On wood surfaces, this may be very useful for preservation properties against aging through the attack of microorganisms, which is currently done by means of lacquering or impregnation. Furthermore, miscellaneous new materials (Maggini et al. 2012) and treatment procedures (Calonego et al. 2012) including chemical bonding (Namyslo and Kaufmann 2009) and nanostructuring of surfaces (Ding et al. 2011) are currently investigated. Since the use of chromated copper arsenate (CCA) and copper chrome boric acid (CCB) is forbidden due to its designation as hazardous materials, some similar approaches were made, trying

to reduce the leaching (Treu et al. 2011; Lesar et al. 2011) and reutilize the materials (Humar et al. 2011). Another field of surface modification is employing laser or plasma technology, which has substantially increased in relevance with regard to wood surfaces during the past few years (Rehn and Viöl 2003; Rehn et al. 2003; Bente et al. 2004; Wolkenhauer et al. 2005, 2009; Kopp et al. 2005; Podgorski et al. 2000; Topala and Dumitrascu 2007; Odraskova et al. 2008; Toriz et al. 2008; Asandulesa et al. 2010; Liu et al. 2010; Busnel et al. 2010).

The treatment of nanoparticle coatings with low-temperature radio frequency plasmas has been found to significantly enhance their durability (Ilic et al. 2010), thus exciting interests for a combined method of plasma-treatment and nanoparticle coating for some industrial applications. These approaches might well be predominant compared to current techniques regarding their economical aspects as well as the improvement of functionality. The combination of both surface treatments is possible in numerous ways, e.g. by using a plasma-jet with precursor gases (Gindrat et al. 2011; Avramidis et al. 2009). To understand the interactions with wood surfaces, several model systems are used to resemble the organic groups of lignin and cellulose. For cellulose these are the molecular precursors cellobiose and glucose. The effect of plasma treatments on these molecules was studied previously (Klarhöfer 2009; Klarhöfer et al. 2010). In the course of that work a significant decrease of carbon–oxygen single bonds was observed during plasma treatments in argon. Along with the accumulation of carbon which is not bound to oxygen, this clearly indicates the reduction of lignin and cellulose at the surface. The fraction of carbon–oxygen double bonds almost does not change (Klarhöfer et al. 2010).

The adsorption behavior of silver on glucose films of different thicknesses was discussed earlier (Dahle et al. 2012). The formation of silver nanoparticles encapsulated in glucose was revealed, while no chemical reactions were found. All of these investigations are part of a research project concerning the interaction of metals (Ag, Ti) with wood surfaces particularly with regard to a preliminary plasma treatment. The results for glucose are employed for the discussion of the recent results on cellobiose and cellulose.

Experimental details

An ultra high vacuum apparatus with a base pressure of 5×10^{-11} hPa, which has been described in detail previously (Maus-Friedrichs et al. 1991; Ochs et al. 1996, 1998; Krischok et al. 2001), is used to carry out the experiments. All measurements were performed at room temperature.

Electron spectroscopy is performed using a hemispherical analyzer (Leybold EA 10) in combination with a source for metastable helium atoms (mainly He* $^3S_1$) and ultraviolet photons (HeI line). A commercial non-monochromatic X-ray source (Fisons XR3E2-324) is utilized for XPS.

During XPS, X-ray photons hit the surface under an angle of 80° to the surface normal, illuminating a spot of several mm in diameter. For all measurements presented here, the Al K_α line with a photon energy of 1,486.6 eV is used. Electrons are recorded by the hemispherical analyzer with an energy resolution of 1.1 eV for detail spectra and 2.2 eV for survey spectra, respectively, under an angle of 10° to the surface normal. All XPS spectra are displayed as a function of binding energy with respect to the Fermi level.

For quantitative XPS analysis, photoelectron peak areas are calculated via mathematical fitting with Gauss-type profiles using OriginPro 7G including the PFM fitting module, which applies Levenberg–Marquardt algorithms to achieve the best agreement between experimental data and fit. To optimize our fitting procedure, Voigt-profiles have been applied to various oxidic and metallic systems but for most systems the Lorentzian contribution converges to 0. Therefore all XPS peaks are fitted with Gaussian shapes. Photoelectric cross sections as calculated by Scofield (1976) with asymmetry factors following Reilman et al. (1976) as well as Powell and Jablonski (2010a) and inelastic mean free paths from the NIST database (Powell and Jablonski 2010b) (using the database of Tanuma, Powell and Penn for elementary contributions and the TPP-2 M equation for molecules) as well as the energy dependent transmission function of our hemispherical analyzer are taken into account when calculating the stoichiometries. According to Klarhöfer et al. (2010), the detail spectra of the C 1s region are analyzed by fitting single Gaussians of equal width for every chemical species. It is assumed to be composed of contributions from

C_1: carbon–carbon or carbon–hydrogen bonds (C–C, C–H),
C_2: carbon–oxygen bonds (C–O),
C_3: carbon linked to two oxygen atoms or twice to one oxygen atom (C=O), (O–C–O) and
C_4: carboxy groups (O=C–O)

For neither of the spectra any contributions of carboxyl groups were found. During the fitting procedure, the relative positions i.e. binding energy differences have been fixed to 1.5 eV for C_1–C_2, 2.8 eV for C_1–C_3, and 3.75 eV for C_1–C_4 according to Nguila Inari et al. (2006).

MIES and UPS are performed applying a cold cathode gas discharge via a two-stage pumping system. A time-of-flight technique is employed to separate electrons emitted by He* (MIES) from those caused by HeI (UPS) interaction with the surface. The combined He*/HeI beam strikes the sample surface under an angle of 45° to the surface normal and illuminates a spot of approximately 2 mm in diameter. The spectra are recorded simultaneously by the hemispherical analyzer with an energy resolution of 220 meV under normal emission within 140 s.

MIES is an extremely surface sensitive technique probing solely the outermost layer of the sample, because the He* atoms interact with the surface typically 0.3–0.5 nm in front of it. This may occur via a number of different mechanisms depending on surface electronic structure and work function, as is described in detail elsewhere (Harada et al. 1997; Morgner 2000; Ertl and Kuppers 1985). Only the processes relevant for the spectra presented here shall be discussed shortly:

During Auger Deexcitation (AD), an electron from the sample fills the 1s orbital of the impinging He*. Simultaneously, the He 2s electron carrying the excess energy is emitted. The resulting spectra reflect the Surface Density of States (SDOS) directly. AD–MIES and UPS can be compared and allow a distinction between surface and bulk effects. AD takes place for all systems shown here.

On pure and partly oxidized metal surfaces with a work function beyond about 3.5 eV, Auger Neutralization (AN) occurs as long as the surface shows metallic behavior. As a result the impinging He^* atom is ionized in the vicinity of the surface by resonant transfer (RT) of its 2s electron in unoccupied metallic surface states. Afterwards, the remaining He^+ ion is neutralized by a surface electron thus emitting a second surface electron carrying the excess energy. The observed electron spectrum is rather structureless and originates from a self convolution of the surface density of states (SDOS).

All MIES and UPS spectra are displayed as a function of the electron binding energy with respect to the Fermi level, thus being able to compare MIES and UPS spectra more easily. Obviously, the binding energy scale is only valid for the AD process. Nevertheless, all spectra including structures originating in the AN process have also been displayed in this particular manner. The surface work function can be determined from the high binding energy onset of the MIES or the UPS spectra with an accuracy of ± 0.1 eV.

Atomic Force Microscopy (AFM) is applied to study the surface topography and to determine the size of the silver nano particles. A Veeco Dimension 3100 SPM is employed to perform the AFM measurements in Tapping Mode. Silicon cantilevers (NSC15 with Al backside coating from Mikromasch) with a resonance frequency of about 308 kHz and a spring constant of about 40 N/m were used together with an optical lever detection technique. All images were gained with a line-scan frequency of 0.5 or 1 Hz, respectively, with 512 pixels for each of the 512 lines. For image postprocessing, SPIP 6.0.9 by Image Metrology A/S is used to level the lines, to remove streaks, peaks and bows. It is also used to smooth the picture with gaussian filter.

The experiments on cellobiose were carried out on inert Au substrates with (111) or (100) crystal surfaces. These substrates have been cleaned prior to the experiments by Ar-sputtering at 3 kV and 5 mA for 60 min and subsequent heating up to 1,000 K. For cellulose, a gold on silicon substrate was cleaned using peroxymonosulfuric acid and afterwards rinsed in deionized water. The Ag reference was prepared by adsorption onto a Si(100) substrate, which was preliminary cleaned by flashing up to 1,400 K.

Silver (Sigma-Aldrich, 99 %) was evaporated with a commercial UHV evaporator (Omicron EFM3) onto the samples. On a clean Si(100) target metallic silver films grow at a rate of 0.23 nm min^{-1} at room temperature when evaporated with an Ag^+ ion flux of 1 μA at the fluxmeter of the EFM3. The film growth rate for Ag has been estimated from the Si 2p peak attenuation in XPS.

D-(+)-Cellobiose (Sigma-Aldrich Co., for microbiology, ≥99.0 %) was evaporated in a directly connected preparation chamber (base pressure $<10^{-9}$ hPa) using a temperature controlled evaporator (Kentax TCE-BS). During all experiments, cellobiose has been evaporated for 3 min at 190 °C. Cellulose (Sigma-Aldrich Co., microcrystalline powder, ca. 20 micron) has been dissolved with 0.5 mg in 10 ml deionized water and afterwards spin-coated on a cleaned Au/Si substrate for 1 min at 17,500 rpm.

Results and discussion

The discussion of the silver adsorption on cellulose will be held basing on the results of the monomer glucose (cf. Dahle et al. 2012) and the dimer cellobiose. Thus, the description of the results starts with silver adsorption on cellobiose and deals with silver on cellulose afterwards.

Silver on cellobiose

Figure 1 shows the MIES and UPS spectra of a cellobiose film before (black lines) and after silver adsorption (red lines). The MIES spectrum of the pristine cellobiose film fits well to previous results on cellobiose (Klarhöfer 2009). It reveals three main structures around 11.5, 10.6 eV and between 8 and 5 eV, which correspond quite well to the structures found for glucose. Similar to the valence band structures of glucose (Dahle et al. 2012), the peaks at 11.5 and 10.6 eV are probably related to the σ-type oxygen state from C–O–H groups in polycarbonate (Dahle et al. 2012; Moliton et al. 1999) and the phenol C 3a″ molecular orbital (MO) in C–H bonds (Dahle et al. 2012; Kimura et al. 1981), respectively. The broad feature between 5 and 8 eV might most likely be due to a π-type MO from C–H bonds like the C 4a″ state of phenol (Dahle et al. 2012; Kimura et al. 1981) for the low binding energy part, while some oxygen 1π state of OH groups (Maus-Friedrichs et al. 2001) or the $1b_1$ state of physisorbed water (Dahle et al. 2012; Günster et al. 2000) may contribute at the high binding energy side. In the UPS spectrum of the pristine cellobiose film, the structures are notably broadened and slightly shifted towards higher binding energies by about 0.5 eV. Nevertheless, the same structures can be found in UPS as described for MIES. After the silver adsorption, the structures remain similar, but are significantly broadened. Furthermore, the work function decreases from 4.5 eV down to about 3.5 eV.

Figure 2 displays XPS spectra of the C 1s regions of a cellobiose film before (black dots) and after adsorption of silver (red dots) as well as the fitted peaks (green lines) and the fit curve (black or red lines) The cellobiose film yields five peaks with the main one corresponding to C–O bonds (C_2). The adjacent peak at the high binding energy side belongs to O–C–O bonds (C_3), while the one at the low binding energy side originates from C–C (C_1). The outermost, minor peaks most probably correspond to aliphatic carbon

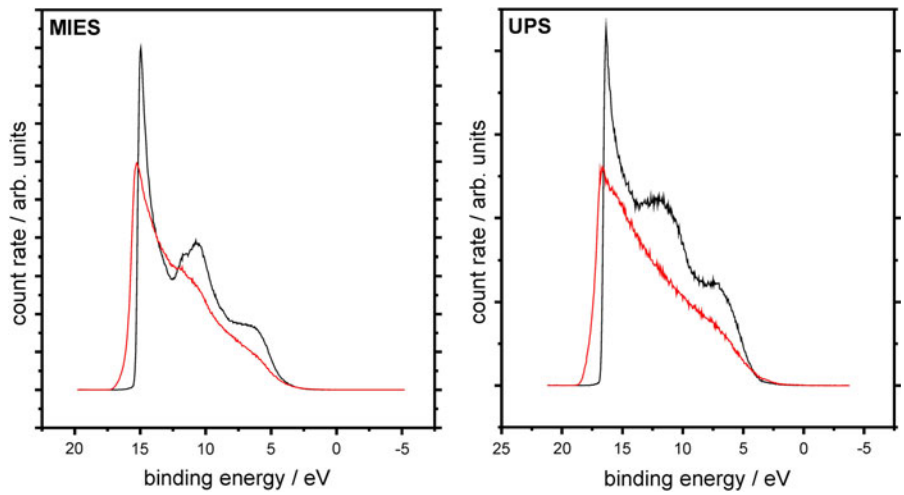

Fig. 1 MIES and UPS spectra of a cellobiose film before (*black lines*) and after silver adsorption (*red lines*). (Color figure online)

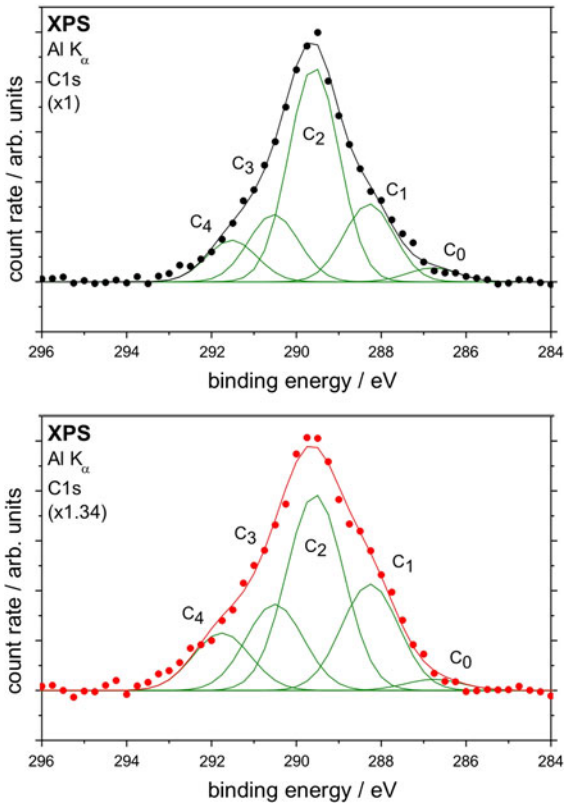

Fig. 2 XPS detail spectra of the C 1s regions of a cellobiose film before (*black dots*, *top* spectrum) and after silver adsorption (*red dots*, *bottom* spectrum) with fitted peaks (*green lines*) and fit curves (*black* or *red line*). (Color figure online)

owing to contamination (C_0) and carboxyl (C_4), respectively. After adsorption of silver the relative intensity of the C–O peak decreases significantly, while the aliphatic and carbonyl groups increase accordingly. Relative intensities, binding energies and full widths at half mean (FWHM) are shown in Tables 1 and 2.

Figure 3 displays XPS detail spectra of the O 1s (top spectra), and Ag 3d (bottom spectra) regions of a cellobiose film before (black dots) and after silver adsorption (red dots). The C 1s and the O 1s spectra of the pristine cellobiose resemble very well the shapes of glucose (Dahle et al. 2012).

For cellobiose, the intensities of the C 1s and O 1s structures get attenuated due to the adsorbed silver. The Ag 3d peak doublet shows no sign of any chemical interaction, while the intensities relative to the C 1s and O 1s peaks are much lower than for the same amount of silver evaporated onto glucose. This might indicate a smaller sticking coefficient for silver

Table 1 XPS fit results for the C 1s region of the as-prepared cellobiose film

Annotation	Binding energy (eV)	FWHM (eV)	Rel. intensity (%)	Correlation
C_0	286.8	1.4	3.4	Residuals
C_1	288.3	1.4	18.7	C–C
C_2	289.6	1.4	51.6	C–O
C_3	290.5	1.4	16.2	O–C–O
C_4	291.5	1.4	10.0	O–C=O

Table 2 XPS fit results for the C 1s region of the silver coated cellobiose film

Annotation	Binding energy (eV)	FWHM (eV)	Rel. intensity (%)	Correlation
C_0	286.8	1.6	2.4	Residuals
C_1	288.3	1.6	23.3	C–C
C_2	289.6	1.6	42.8	C–O
C_3	290.5	1.6	18.9	O–C–O
C_4	291.8	1.6	12.6	O–C=O

on cellobiose than for silver on glucose on the one hand, or adsorption sites deeper down inside the cellobiose film than in the glucose film. All stoichiometries and C/O-ratios are given in Table 5.

Figure 4 decipts an AFM picture of cellobiose with adsorbed silver on Au(111). The microdroplet like topopraphy (c.f. Dahle et al. 2012) has been flattened by a 5th order polynomial fit to work out the nanoparticles on top. The picture has a range of 1 μm × 1 μm with a height range of 150 nm, while the not-flattened image has a range of about 650 nm. The most nanoparticles have a diamater of about (350 ± 175) nm and a height of about (25 ± 5) nm.

Figure 5 shows an AFM picture in a range of 5 μm × 5 μm in a height range of 600 nm. The image is taken at a vicinal part of the Au(100) substrate, giving rise to a high density of terrace edges that can be seen in the middle part of the displayed region. On top of these terraces are two different kinds of particles. The bigger ones have a diameter of (750 ± 250) nm and a height range of (125 ± 35) nm. The smaller particles have a diameter of circa (190 ± 40) nm and a height range of (40 ± 8) nm. At both sides of the regions, the gold terraces are covered by a droplet-shaped film of cellobiose. Assuming a distribution of

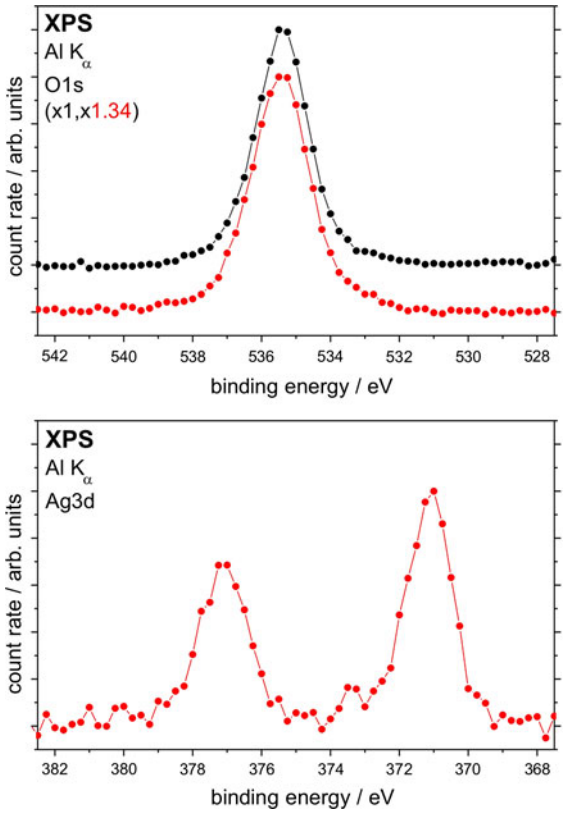

Fig. 3 XPS detail spectra of the O 1s (*top* spectra) and Ag 3d (*bottom* spectra) regions of a cellobiose film before (*black dots*) and after silver adsorption (*red dots*). (Color figure online)

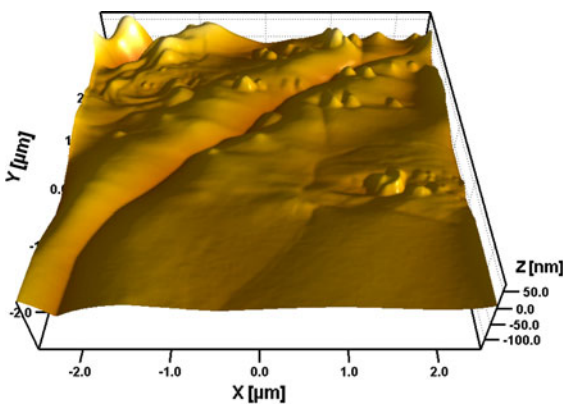

Fig. 4 AFM image of cellobiose after silver adsorption and contact to air, flattened by a 5th order polynomial fit of an area of 1 µm × 1 µm with a height range of 150 nm

terrace edges beneath the droplets that are comparable to the visible ones, the film may have a thickness of about 200 nm.

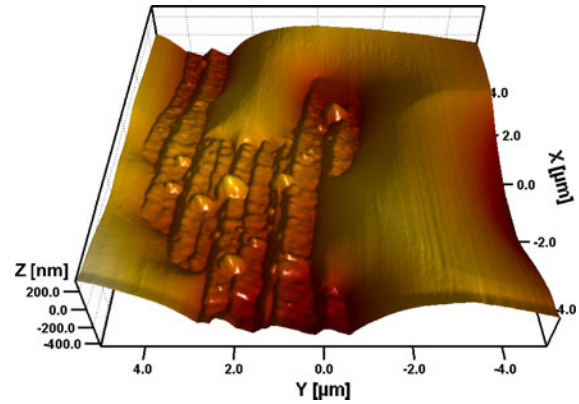

Fig. 5 AFM image of a region of 5 µm × 5 µm in a height range of 600 nm of the same film as Fig. 3 at a vicinal part of the Au(100) substrate

Silver on cellulose

Figure 6 exhibits MIES and UPS spectra of a cellulose film before (black lines) and after silver adsorption (red lines). The spectra after silver adsorption have been scaled up for better visibility by a factor of 5 in MIES and a factor of 2 in UPS. Because of the heavy noise in UPS, both spectra have been smoothened by a moving average over an interval of five values. The valence band features of the pristine cellulose film are broadened even more than the features of cellobiose. The binding energies correspond very well to those found for glucose (Dahle et al. 2012) and do not show any shift in contrast to cellobiose (see "Silver on cellobiose" section). The intensity at the very left side of the spectra is due to a slight electrical charging of the cellulose film. The absence of any gold structures indicates a completely covered substrate, even though optical microscopy revealed a sparse distribution of cellulose microcrystals. This could potentially be due to a salvation-precipitation-mechanism of short-chained cellulose molecules. After the silver adsorption, the valence band features of the cellulose and the work function of 4.4 eV remain unaffected, whereas the secondary electron peak decreases significantly. The additional structure between 4 and 7 eV in the UPS spectrum can be identified as Ag 4d. The surplus intensity between 6 and 8 eV as well as the increased shoulder below 5 eV in MIES are most probably due to the Ag AN feature, a convolution of the Ag 4d and Ag 5s orbitals (Stracke et al. 2001; Heinz and Morgner 1997).

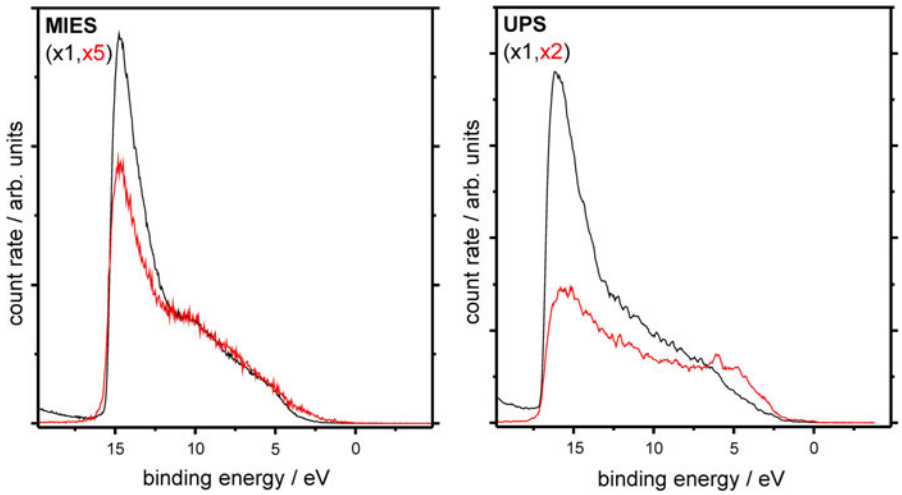

Fig. 6 MIES and UPS spectra of a cellulose film before (*black lines*) and after silver adsorption (*red lines*). (Color figure online)

In order to prove that the silver structures found in the MIES spectrum correspond to the AN process rather than the AD process, the possible energies for different electron emissions from silver surfaces have been calculated. We assume an electron from a state with binding energy E_{rel} to fill the He 1s orbital. The kinetic energy E_{kin} of the simultaneously emitted second electron with a binding energy E_{em} off a sample with work function Φ can then be written as

$$E_{kin} = IP - E_{rel} - E_{em} - \Phi \quad (1)$$

The kinetic energy of these electrons would calculate into binding energies of

$$E_B = 19.8\,eV - E_{kin} \quad (2)$$

In the case of both electrons originating in the Ag 4d band with its maximum around 4.5 eV and a work function of 4.4 eV as estimated from the present measurements (c.f. Fig. 6), the energies calculate to

$$E_{kin} = 24.6\,eV - 4.5\,eV - 4.5\,eV - 4.4\,eV = 11.2\,eV, \quad (3a)$$

$$E_B = 19.8\,eV - 11.2\,eV = 8.6\,eV. \quad (3b)$$

If the first electron originates from the Ag 4d and the emitted electron from the Ag 5s orbital with a mean binding energy of about 2 eV adds up to

$$E_{kin} = 24.6\,eV - 4.5\,eV - 2.0\,eV - 4.4\,eV = 13.7\,eV, \quad (4a)$$

$$E_B = 19.8\,eV - 13.7\,eV = 6.1\,eV. \quad (4b)$$

In the case of both electrons originating in th Ag 5s band with its means binding energy of about 2 eV results in an AN–MIES structure at

$$E_{kin} = 24.6\,eV - 2.0\,eV - 2.0\,eV - 4.4\,eV = 16.2\,eV, \quad (5a)$$

$$E_B = 19.8\,eV - 16.2\,eV = 3.6\,eV. \quad (5b)$$

Figure 7 displays XPS spectra of the C 1s regions of a cellulose film before (black dots) and after adsorption of silver (red dots) as well as the fitted peaks (green lines) and the fit curve (black or red lines). These structures contain five peaks just like the cellobiose film. Compared to cellobiose, the amount of C–O groups (C_2) is smaller and after adsorption of silver, the intensity of the C–O peak decreases significantly, while mainly carbonyl and carboxyl groups increase. Relative intensities, binding energies and widths are shown in Tables 3 and 4.

Figure 8 presents XPS detail spectra of the O 1s (top spectra)and Ag 3d (bottom spectra) regions of a cellulose film before (black dots) and after silver adsorption (red dots). The C 1s (Fig. 7) and O 1s spectra of the pristine cellulose film resemble very well the spectra of glucose (Dahle et al. 2012) and cellobiose (see "Silver on cellobiose" section) except for a shoulder at the low binding energy side. After the silver adsorption, the intensity of these structures get attenuated due to the adsorbed film. The Ag 3d peak doublet appearing after silver adsorption shows just contents of metallic silver without any trace of chemical interactions with the cellulose film. All stoichiometries and C/O-ratios are given in Table 5.

Figure 9 exhibits an AFM image of a clean Au/Si substrate. The region of 1 μm × 1 μm includes a height range of only 12.8 nm. The whole gold film on the silicon substrate is found to consist of

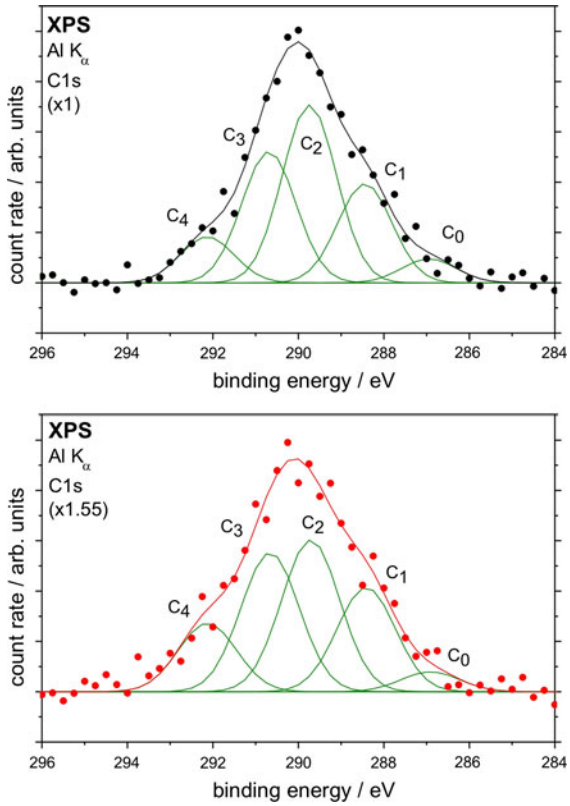

Fig. 7 XPS detail spectra of the C 1s regions of a cellulose film before (*black dots*, *top* spectrum) and after silver adsorption (*red dots*, *bottom* spectrum) with fitted peaks (*green lines*) and fit curves (*black* or *red line*). (Color figure online)

Table 3 XPS fit results for the C 1s region of the as-prepared cellulose film

Annotation	Binding energy (eV)	FWHM (eV)	Rel. intensity (%)	Correlation
C_0	286.9	1.5	5.0	Residuals
C_1	288.4	1.5	20.7	C–C
C_2	289.7	1.5	37.2	C–O
C_3	290.7	1.5	27.4	O–C–O
C_4	292.1	1.5	9.6	O–C=O

nanoparticles with diameters in the order of magnitude of 100 nm.

Figure 10 displays an AFM image of cellulose on an Au/Si substrate with adsorbed silver. It has a range of 1 μm × 1 μm and a height range of 400 nm. One can see a crest-like structure as well as a rather rough,

Table 4 XPS fit results for the C 1s region of the silver coated cellulose film

Annotation	Binding energy (eV)	FWHM (eV)	Rel. intensity (%)	Correlation
C_0	286.9	1.6	4.1	Residuals
C_1	288.4	1.6	21.6	C–C
C_2	289.7	1.6	31.4	C–O
C_3	290.7	1.6	28.8	O–C–O
C_4	292.1	1.6	14.1	O–C=O

cloudy structure on the right hand side. This cloudy structure corresponds very well to the particle based shape that was found for the underlying Au/Si substrate (see Fig. 9). The cellulose crest structure exhibits no sign of silver particle formation like glucose (c.f. Dahle et al. 2012) or cellobiose (see Silver on cellobiose" section).

Figure 11 shows an AFM image of another region of the silver coated cellulose film shown in Fig. 9. The lateral range amounts to 1 μm × 1 μm with a height range of 80 nm. The surface reproduces the cloudy structure as in Fig. 9 very well, even though a slight broadening of the initially found particles on the gold film indicates the deposition of short-chained cellulose molecules over the whole sample.

Discussion

The spectroscopic results yield a nice reproduction of the valence band states known from glucose for both, the dimer cellobiose as well as the polymer cellulose. The adjacent adsorption of silver did not lead to any reaction or other chemical interaction at all. Regarding the microscopic results for cellobiose, large micro-droplets were found which were exhibiting nanoparticles on top equally to those previously found on glucose. On the other hand, none of these particles could be found on cellulose. Even though it was not possible to picture the surface of the cellulose microcrystals with AFM, similar nanoparticles should also have been formed on the cellulose hillocks (see "Silver on cellulose" section). Since there is no sign of silver nanoparticles, any formation of them can mostly be excluded. The coverage of the glucose film with silver nanoparticles enclosed in glucose was attributed to the known interaction of the glucose's OH groups

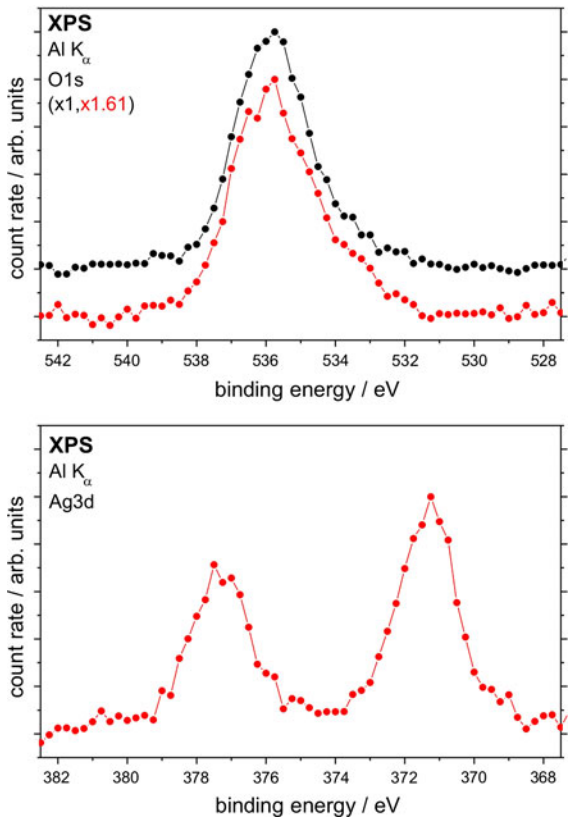

Fig. 8 XPS detail spectra of the O 1s (*top* spectra) and Ag 3d (*bottom* spectra) regions of a cellulose film before (*black lines*) and after silver adsorption (*red lines*). (Color figure online)

Table 5 Stoichiometries and carbon/oxygen-ratios for all samples as calculated from the XPS results

Sample	at.% C	at.% O	at.% Ag	C/O
Cellobiose	75.84	24.16	–	3.14
Ag/cellobiose	74.70	21.81	3.49 %	3.43
Cellulose	74.03	25.97	–	2.85
Ag/cellulose	71.73	24.57	3.70 %	2.92

with silver, which is usually reported to be the competing process to the oxidation of the glucose at least in the case of silver ions (c.f. Venediktov et al. 2012 and Janardhanan et al. 2009). This oxidation effect has also been observed for cellobiose and cellulose as described in "Silver on cellobiose" section and "Silver on cellulose" section. While the formation of likewise structures on cellobiose indicates the exactly same kind of interaction found for silver adsorption on glucose films in a previous study (Dahle et al. 2012), the long cellulose polymer is most

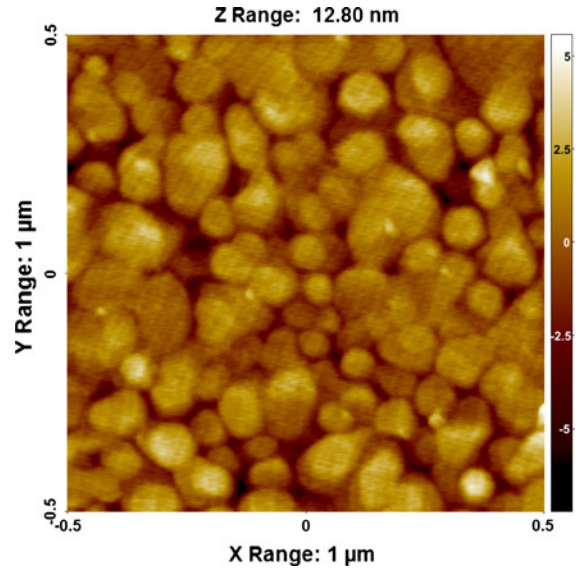

Fig. 9 AFM image of a 1 µm × 1 µm region with a height range of 12.8 nm of a cleaned Au/Si substrate

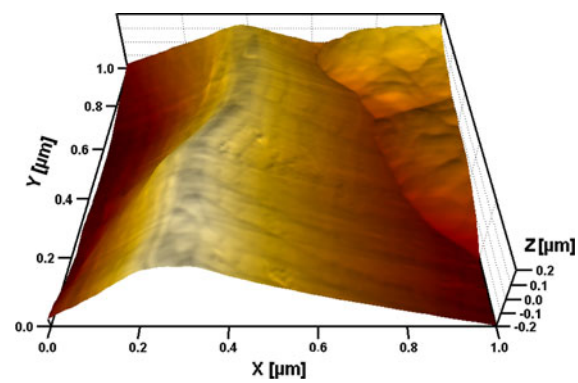

Fig. 10 AFM image of a 1 µm × 1 µm region with a height range of 400 nm of cellulose on Au/Si after silver adsorption

probably not able to surround the adsorbed silver in a similar way due to geometrical and mobility reasons. On the other hand, the spectroscopic measurements reveal an adsorption site near to the surface of the cellulose. Thus, the absence of silver nanoparticles suggests an interaction between the cellulose molecules and the silver atoms at energies high enough to overcome the interaction between silver atoms, since it should otherwise lead to agglomeration. This adhesion for silver atoms upon adsorption should at least also be partly present for silver nanoparticles and hence stabilize a coating of cellulose based materials with such particles.

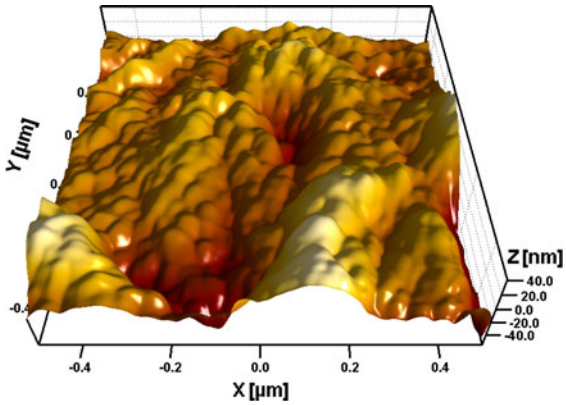

Fig. 11 AFM image of a 1 µm × 1 µm region with a height range of 80 nm of cellulose on Au/Si after silver adsorption (c.f. Fig. 7)

Conclusions

The silver adsorption experiments on cellobiose reveals the formation of silver clusters encapsulated in a film of cellobiose without further chemical reactions, similar to previous findings for glucose (Dahle et al. 2012). The cellulose film on the other hand did not lead to the formation of nanoparticles upon silver adsorption, suggesting that the energy for the adsorption of silver has to be larger than for the interaction between silver atoms. Thus, cellulose is proposed to stabilize silver nanoparticle coatings.

Acknowledgments We thankfully acknowledge the provision of the Atomic Force Microscope by the group of Prof. W. Daum (Institut für Energieforschung und Physikalische Technologien, TU Clausthal) as well as the technical assistance of Lienhard Wegewitz and Dana Schulte Genannt Berthold. Finally, we thank the Deutsche Forschungsgemeinschaft (DFG) for financial support under Project Numbers MA 1893/18-1 and VI 359/9-1.

References

Asandulesa M, Topala I, Dumitrascu N (2010) Effect of helium DBD plasma treatment on the surface of wood samples. Holzforschung 64:223–227. doi:10.1515/hf.2010.025

Avramidis G, Wolkenhauer A, Zhen B, Militz H, Viöl W (2009) Water repellent coatings on wood surfaces generated by a dielectric barrier discharge plasma jet at atmospheric pressure. Proceedings of the European conference on wood modification

Bente M, Avramidis G, Förster S, Rohwer EG, Viöl W (2004) Wood surface modification in dielectric barrier discharges at atmospheric pressure for creating water repellent characteristics. Holz Roh Werkst 62:157–163. doi:10.1007/s00107-004-0475-0

Busnel F, Blanchard V, Prégent J, Stafford L, Riedl B, Blanchet P, Sarkissian A (2010) Modification of sugar maple (*Acer saccharum*) and black spruce (*Picea mariana*) wood surfaces in a dielectric barrier discharge (DBD) at atmospheric pressure. J Adhes Sci Technol 24:1401–1413. doi:10.1163/016942410X501007

Calonego FW, Severo ETD, Ballarin AW (2012) Physical and mechanical properties of thermally modified wood from *E. grandis*. Eur J Wood Prod 70:453–460. doi:10.1007/s00107-011-0568-5

Dahle S, Meuthen J, Viöl W, Maus-Friedrichs W (2012) Adsorption of silver on glucose studied with MIES, UPS, XPS and AFM. Appl Surf Sci. doi:10.1016/j.apsusc.2013.07.126

Ding X, Richter DL, Matuana LM, Heiden PA (2011) Efficient one-pot synthesis and loading of self-assembled amphiphilic chitosan nanoparticles for low-leaching wood preservation. Carbohyd Polym 86:58–64. doi:10.1016/j.carbpol.2011.04.002

El-Shishtawy RM, Asiri AM, Abdelwahed NAM, Al-Obtaibi MM (2011) In situ production of silver nanoparticle on cotton fabric and its antimicrobial evaluation. Cellulose 18:75–82. doi:10.1007/s10570-010-9455-1

Ertl G, Kuppers J (1985) Low energy electrons and surface chemistry. VCH, Weinheim

Gindrat M, Höhle HM, von Niessen K, Guittienne Ph, Grange D, Hollenstein Ch (2011) Plasma spray-CVD: a new thermal spray process to produce thin films from liquid or gaseous precursors. J Therm Spray Techn 20:882–887. doi:10.1007/s11666-011-9655-8

Günster J, Krischok S, Stultz J, Goodman DW (2000) Interaction of Na with multilayer water on MgO(100). J Phys Chem B 104:7977–7980. doi:10.1021/jp001375+

Harada Y, Masuda S, Ozaki H (1997) Electron spectroscopy using metastable atoms as probes for solid surfaces. Chem Rev 97:1897–1952. doi:10.1021/cr940315v

Heinz B, Morgner H (1997) MIES investigation of alkanethiol monolayers self-assembled on Au(111) and Ag(111) surfaces. Surf Sci 372:100–116. doi:10.1016/S0039-6028(96)01131-4

Humar M, Budija F, Hrastnik D, Lesar B, Petrič M (2011) Potentials of liquefied CCB treated waste wood for wood preservation. Drvna Industrija 62:213–218

Ilic V, Saponjic Z, Vodnic V, Lazovic S, Dimitrijevic S, Jovancic P, Nedeljkovic JM, Radetic M (2010) Bactericidal efficiency of silver nanoparticles deposited onto radio frequency plasma pretreated polyester fabrics. Ind Eng Chem Res 49:7287–7293. doi:10.1021/ie1001313

Janardhanan R, Karuppaiah M, Hebalkar N, Rao TN (2009) Synthesis and surface chemistry of nano silver particles. Polyhedron 28:2522–2530. doi:10.1016/j.poly.2009.05.038

Kimura K, Katsumata S, Achiba Y, Yamazaki T, Iwata S (1981) Handbook of HeI Photoelektron spectra of fundamental organic molecules. Japan Scientific Societies Press, Tokyo and Halsted Press, New York

Klarhöfer L (2009) Elektronenspektroskopische Untersuchungen an funktionalisiertem Holz und Holzbestandteilen. PhD thesis at the Clausthal University of Technology, ISBN 978-3-940394-74-3

Klarhöfer L, Viöl W, Maus-Friedrichs W (2010) Electron spectroscopy on plasma treated lignin and cellulose. Holzforschung 64:331–336. doi:10.1515/hf.2010.048

Kopp M, Roddewig E, Günther H, Ohms G, Leck M, Viöl W (2005) 157 nm fluorine laser ablation of wooden surfaces as an improved preparation technique for microscopy. Laser Phys Lett 2:16–20. doi:10.1002/lapl.200410143

Krischok S, Höfft O, Günster J, Stultz J, Goodman DW, Kempter V (2001) H_2O interaction with bare and Li-precovered TiO_2: studies with electron spectroscopies (MIES and UPS(HeI and II)). Surf Sci 495:8–18. doi:10.1016/S0039-6028(01)01570-9

Lesar B, Ugovsek A, Kariz M, Sernek M, Humar M, Kralj P (2011) Influence of boron compounds in adhesives on the bonding quality and fungicidal properties of wood. Wood Res Slovakia 56:385–392

Liu Y, Tao Y, Lv X, Zhang Y, Di M (2010) Study on the surface properties of wood/polyethylene composites treated under plasma. Appl Surf Sci 257:1112–1118. doi:10.1016/j.apsusc.2010.08.032

Lok CN, Ho CM, Chen R, He QY, Yu WY, Sun H, Tam PKH, Chiu JF, Che CM (2006) Proteomic analysis of the mode of antibacterial action of silver nanoparticles. J Proteome Res 5:916–924. doi:10.1021/pr0504079

Maggini S, Feci E, Cappelletto E, Girardi F, Palanti S, DiMaggio R (2012) (I/O) hybrid alkoxysilane/zirconium-oxocluster copolymers as coatings for wood protection. Appl Mater Interfaces 4:4871–4881. doi:10.1021/am301206t

Maus-Friedrichs W, Dieckhoff S, Kempter V (1991) Alkali-metal-affected adsorption of CO on W(110) studied by metastable impact electron spectroscopy. Surf Sci 249:149–158. doi:10.1016/0039-6028(91)90840-O

Maus-Friedrichs W, Gunhold A, Frerichs M, Kempter V (2001) The interaction of CO_2 and H_2O with Sr films studied with MIES und UPS (HeI). Surf Sci 488:239–248. doi:10.1016/S0039-6028(01)01140-2

Moliton JP, Jussiaux-Devilder C, Trigaud T, Lazzaroni R, Bredas JL, Galaup S, Kihn Y, Sevely J (1999) Plasmons as the primary mechanism of ion-induced modifications in polymers. Philos Mag B 79:793–815. doi:10.1080/01418639925710 4

Morgner H (2000) The characterization of liquid and solid surfaces with metastable helium atoms. Adv At Mol Opt Phys 42:387–488. doi:10.1016/S1049-250X(08)60191-3

Namyslo JC, Kaufmann DE (2009) Chemical improvement of surfaces. Part 1: novel functional modification of wood with covalently bound organoboron compounds. Holzforschung 63:627–632. doi:10.1515/HF.2009.112

Nguila Inari G, Petrissans M, Lambert J, Ehrhardt JJ, Gérardin P (2006) XPS characterization of wood chemical composition after heat-treatment. Surf Interface Anal 38:1336–1342. doi:10.1002/sia.2455

Ochs D, Maus-Friedrichs W, Brause M, Günster J, Kempter V, Puchin V, Shluger A, Kantorovich L (1996) Study of the surface electronic structure of MgO bulk crystals and thin films. Surf Sci 365:557–571. doi:10.1016/0039-6028(96)00706-6

Ochs D, Brause M, Braun B, Maus-Friedrichs W, Kempter K (1998) CO_2 chemisorption at Mg and MgO surfaces: a study with MIES and UPS (He I). Surf Sci 397:101–107. doi:10.1016/S0039-6028(97)00722-X

Odraskova M, Rahel J, Zahoranova A, Tino R, Cernak M (2008) Plasma activation of wood surface by diffuse coplanar surface barrier discharge. Plasma Chem Plasma P 28:203–211. doi:10.1007/s11090-007-9117-8

Podgorski L, Chevet B, Onic L, Merlin A (2000) Modification of wood wettability by plasma and corona treatments. Int J Adhes Adhes 20:103–111. doi:10.1016/S0143-7496(99)00043-3

Powell CJ, Jablonski A (2010a) Progress in quantitative surface analysis by X-ray photoelectron spectroscopy: current status and perspectives. J Electron Spectrosc Relat Phenom 178:331–346. doi:10.1016/j.elspec.2009.05.004

Powell CJ, Jablonski A (2010b) NIST electron inelastic-mean-free-path database—version 1.2. National Institute of Standards and Technology, Gaithersburg, MD. http://www.nist.gov/srd/nist71.cfm

Rehn P, Viöl V (2003) Dielectric barrier discharge treatments at atmospheric pressure for wood surface modification. Holz Roh Werkst 61:145–150. doi:10.1007/s00107-003-0369-6

Rehn P, Wolkenhauer A, Bente M, Förster S, Viöl W (2003) Wood surface modification in dielectric barrier discharges at atmospheric pressure. Surf Coat Tech 174–175:515–518. doi:10.1016/S0257-8972(03)00372-4

Reilman RF, Msezane A, Manson ST (1976) Relative intensities in photoelectron spectroscopy of atoms and molecules. J Electron Spectrosc Relat Phenom 8:389–394. doi:10.1016/0368-2048(76)80025-4

Scofield JH (1976) Hartree-Slater subshell photoionization cross-sections at 1254 and 1487 eV. J Electron Spectrosc Relat Phenom 8:129–137. doi:10.1016/0368-2048(76)80015-1

Stracke P, Krischok S, Kempter V (2001) Ag-adsorption on MgO: investigations with MIES and UPS. Surf Sci 473:86–96. doi:10.1016/S0039-6028(00)00956-0

Topala I, Dumitrascu N (2007) Dynamics of the wetting process on dielectric barrier discharge (DBD)-treated wood surfaces. J Adhes Sci Technol 21:1089–1096. doi:10.1163/156856107782105936

Toriz G, Gutierrez MG, Gonzalez-Alvarez V, Wendel A, Gatenholm P, Martinez-Gomez AD (2008) Highly hydrophobic wood surfaces prepared by treatment with atmospheric pressure dielectric barrier discharges. J Adhes Sci Technol 22:2059–2078. doi:10.1163/156856108X332561

Treu A, Larnøy E, Militz H (2011) Process related copper leaching during a combined wood preservation process. Eur J Wood Prod 69:263–269. doi:10.1007/s00107-010-0427-9

Venediktov EA, Ganiev ARF, Padokhin VA (2012) Mechanism of formation of silver nanoparticle ensembles in an aqueous solution of glucose. Dokl Chem 442:34–36. doi:10.1134/S0012500812020085

Wolkenhauer A, Meiners A, Rehn P, Avramidis G, Leck M, Viöl W (2005) Haftverbesserung von Holzbeschichtungen durch Plasma-Vorbehandlung. Holztechnologie 46:40–47

Wolkenhauer A, Avramidis G, Hauswald E, Militz H, Viöl W (2009) Sanding versus plasma treatment of aged wood: a comparison with respect of surface energy. Int J Adhes Adhes 29:18–22. doi:10.1016/j.ijadhadh.2007.11.001

Xue CH, Chen J, Yin W, Jia ST, Ma JZ (2012) Temperature-dependent ferroelectric and dielectric properties of $Bi_{3.25}La_{0.75}Ti_3O_{12}$ thin films. Appl Surf Sci 256:2468–2472. doi:10.1016/j.apsusc.2009.10.089

Yang KY, Choi KC, Ahn CW (2009) Surface plasmon-enhanced energy transfer in an organic light-emitting device structure. Opt Express 17:11495–11504. doi:10.1364/OE.17.011495